Energy Conversion and Management, Volume 277, February 2023, Article number 116597
DOI: 10.1016/j.enconman.2022.116597

This is the pre-print version of our paper which has been accepted for publication in

Energy Conversion and Management

[2023, Vol. 277, p. 116597, (doi: https://doi.org/10.1016/j.enconman.2022.116597)]

Thermodynamics Analysis of a Novel Absorption Heat Transformer-Driven Combined Refrigeration and Desalination System

Ravi Beniwal [a], Kapil Garg [b], Himanshu Tyagi [a,*]

[a] Department of Mechanical Engineering, Indian Institute of Technology Ropar, Rupnagar - 140001, Punjab, India

[b] Centre for Thermal Energy and Materials (CTEM), School of Water, Energy and Environment (SWEE), Cranfield University, Cranfield, Bedfordshire MK43 0AL, UK

Email(s): ravi.20mez0013@iitrpr.ac.in, kapil.garg@cranfield.ac.uk, tyagi.himanshu@gmail.com & himanshu.tyagi@iitrpr.ac.in

* Corresponding author, Phone: +91-1881-232363

NOMENCLATURE

English Symbols

$\dot{E}$	Exergy rate [kW]
h	Specific enthalpy [kJ/kg]
$\dot{H}$	Enthalpy rate [kW]
$\dot{m}$	Mass flow rate of solution inside absorption system [kg/sec]
$\dot{M}$	Mass flow rate [kg/sec]
$\dot{M}_r$	Mass flow rate ratio [--]
p	Pressure [Pa]
$\dot{Q}$	Heat transfer rate [kW]
s	Entropy [kJ/kg-K]
s_o	Reference Entropy[kJ/kg-K]

T	Temperature [^{o}C]
T_o	Reference temperature [^{o}C]
X	Mass fraction in liquid phase [--]
Y	Mole fraction in gaseous phase [--]

Subscripts

a	Dry air
Abs	Absorber
Cond	Condenser
d	Distillate
D	Destruction
des	Desorber
DH	Dehumidifier
*ev*ap	Evaporator
f	Feed
fg	Latent
G	Gas
H	Humidifier
i	Inlet
L	Liquid
max	maximum
o	Outlet
*rec*t	Rectifier
sol	Solution
w	Water

Superscript

CE	Chemical exergy
KN	Kinetic exergy
PE	Physical exergy
PT	Potential exergy

Greek letters

Δ	Difference
ε	Effectiveness
Σ	Summation
ω	Humidity ratio

Abbreviations

AHT	Absorption heat transformer
CAOW	Closed air open water
CCHP	Combined cooling, heating and power
COP	Coefficient of performance
CSP	Concentrated solar power
EES	Energy equation solver
GOR	Gain output ratio
GTL	Gross temperature lift
HDH	Humidification-dehumidification
MED	Multi-effect distillation
OAOW	Open air open water
PR	Performance ratio
SEC	Specific energy consumption
SHX	Sensible heat exchanger
SWH	Solar water heater
TSTEC	Total specific thermal energy consumption
VAHT	Vapour absorption heat transformer
VARS	Vapour absorption refrigeration system

Abstract

Preservation of food and medicines below sub-zero temperatures is the need of the present times. To achieve the required temperature using renewable energy, a waste heat-driven vapour absorption refrigeration system can be implemented. Majority of the available waste heat is

available in the low temperature range i.e. between 60-80ºC, which cannot be directly used to provide refrigeration. Therefore, an absorption heat transformer (AHT) is coupled with the VARS (Vapour absorption refrigeration system) system which increases temperature of this waste heat, and the upgraded heat is utilized to produce required refrigeration effect. Further, the rectifiers' waste heat of the absorption system will be used to power humidification-dehumidification (HDH) desalination cycle. Although all these three components (AHT, VARS, and HDH) have been studied individually, but they have never been combined altogether. This paper presents a mathematical model for the proposed system and its validation against published available literature. The performance parameters such as coefficient of performance, gain output ratio and refrigeration effect of the system is evaluated at different evaporator and desorber temperatures. For 300kW waste heat at 80ºC, evaporator (VARS) temperature of -10ºC, the system reported 70kW of refrigeration effect is provided with 20kg/hr of distillate production rate. An exergy destruction of 82.64 kW has been reported for total input exergy of 142.2 kW, for refrigeration capacity of 157 kW.

Keywords:
Vapour absorption refrigeration, Humidification-dehumidification, Desalination, Waste heat, Gain output ratio, Upgraded heat.

1. Introduction

Due to rapid growth in population and limited food and medicine production, it has become necessity to preserve these under controlled environmental conditions. Transportation of these items cannot be done under ambient conditions; otherwise, fouling and deterioration will occur. To maintain their shelf life for an extended period, preservation under a specified temperature condition is necessary [1]. Conventionally, fossil fuel-driven technology runs the preservation system for its controlled storage but due to its limited availability and also high carbon footprint we are shifting towards renewable based technologies [2].

Also, the lack of potable water for the increasing population is a factor of concern. Over the past few decades, to overcome the scarcity of potable water, seawater desalination has been extensively performed. But there is a problem associated with the already used technology, i.e. the

commercially available desalination technologies require a huge amount of energy which is supplied using burning fossil-fuels [3]. Therefore, to overcome this problem and to decentralize the water supply, a waste heat driven humidification-dehumidification desalination system can be used as it is considered to be an ideal technology for those regions where demand for freshwater is at small scale (1-100 m^3/day) and decentralized [4].

Several combinations of absorption heat transformer (AHT), vapour absorption refrigeration system (VARS) and humidification-dehumidification (HDH) desalination system are reported in the literature for better utilization of the supplied waste heat. Absorption heat transformer upgrades the waste heat by utilizing the heat of absorption released during the absorption of refrigerant in the absorber, kept at higher pressure of the AHT system. In VARS and AHT system, sorbers play a key role in determining the performance of the system. Table 1 presents a summary of study of sorbers in the absorption systems.

Table 1: Summary of study of sorbers in the absorption systems.

Absorber type	Working fluid	Results	Reference
Falling film	LiBr–H2O with n-octanol	• Compared with the bared tube, the micro hatched system performance is improved by a factor of 4.5. • The dominance on the heat transfer is more due to the inclusion of additive than the microstructures	Park et al., 2004, [5]
	NH_3-H_2O	• Performed numerical modelling and experimental analysis using plate heat exchanger was used. • The detailed analysis helps to understand the temperature and mass fraction variation at absorber outlet.	Triché et al., 2016 [6]
	LiBr-H_2O	• A high absorption rate of 0.007 kg/s-m^2 was achieved. • The rate of absorption is inversely proportional to the temperature of the heat transfer fluid.	Michel et al., 2017 [7]
	NH3–H20 with	• For the 15 % mass fraction of ammonia, the rate of absorption ratio was increased by 50 % and 0 % for ZnFe2O4 and Fe2O3.	Yang et al., 2011, [8]

	ZnFe2O4, Fe2O3	• A decrease in the viscosity of the nanofluid and increase in the heat transfer rate leads to higher absorption capacity.	
	LiBr–H2O with SiO2; S:2E1H VT	• For 0.005% concentration of SiO2 nanoparticles, the improvement in the heat and mass transfer coefficients reported to be 46.8 and 18 %. • Nanoparticles outperforms the thermal performance of the system compared to te combination of nanoparticles and surfactant.	Kim et al., 2012, [9]
	LiBr–H2O with Fe (III) Nano powder Adiabatic	• For the flow rate of 3 and 3.5 L/min of the nanofluid, the increase in the absorption rate was 17.6 and 4.9 %. • An external magnetic field further enhances the rate of absorption.	Wu and Rincon Ortiz, 2020, [10]
Bubble	R124-DMAC	• Limiting the solution and the cooling water supply temperature leads to higher rates of absorption capacity. • A 1.87 mm orifice diameter produces more optimal results in terms of absorption capacity.	Jiang et al., 2017, [11]
	NH_3-H_2O	• A helical screw type mixer shows an improvement of 36.61% in the absorption rate over the conventional tube system.	Cerezo et al., 2018 [12]
	NH_3-$LiNO_3$	• They obtained a heat transfer and mass transfer coefficient in the range of 0.9 – 1.8 kW/m^2K and 0.036 – 0.059 m/s. • The increase in the effective length can lead to a higher rate of absorption.	Chan et al., 2018 [13]
	R134a–DMAC	• There is a reduction in the bubble column height in the range of 7-45% fort a raise in the frequency up to 25 Hz.	Wu et al., 2019, [14]
	R124-NMP	• The rate of heat and mass transfer increases for the increase in the Reynold number and the absorption pressure, while it decreases for an increase in the orifice diameter.	Wang et al., 2020, [15]
Membrane	LiBr-H_2O	• Results show high absorption rate equivalent to 100 μm film with two order reduced pressure drop by introducing microstructures in the flow channels.	Nasr Isfahani et al., 2015 [16]

LiBr-H_2O	• Increased irreversibility due to an increase in the feed temperature leads to sudden decreased adiabatic temperature and increased mass flux..	Hong et al., 2018 [17]
LiBr-H_2O	• The new design leads to more uniform film layer. • They reported twice the rate of absorption rate when compared with the conventional type of falling film type absorber.	Mortazavi et al., 2015 [18]

Wang et al. [19] proposed pinch-point based selection criteria for heat pumps and AHT working on available low-grade waste heat. Liang et al. [20] focused on enriching the thermal performance of a ground heat exchanger by improving the material and the thermophysical properties of tee heat exchanger. The heat from the ground heat exchanger is used to drive a heat pump which includes a major electricity consuming equipment, i.e. compressor. Valles et al. [21] proposed a system which provides both cooling (from VARS) and heating (from AHT) according to the requirement by changing the flow direction. A temperature lift of 60oC was also reported for the evaporator temperature of 75oC and condenser temperature of 38oC at 600 kW of solar radiation [22]. Generally the waste heat temperatures that are used as a heat source in the AHY varied from 55oC to 120oC, depending upon the condenser and the evaporator temperature [23].

Further hybridization of the cycles reduces the number of components and the loss of exergy associated with it. Hong et al. [24] proposes a hybrid absorption cycle containing a sub-heat pump and a sub-refrigeration cycle. The refrigerant from the condenser is distributed accordingly to meet the required cooling and heating. The overall cycle COP was reported to be 0.60. Using this lower temperature waste heat and still reaching the desired higher output temperatures can be achieved by integrating chemisorption and mechanical compression step in a single hybrid heat pump concept [25]. Further, an AHT driven combined cooling, heating and power (CCHP) system shows an improvement of 27.98 %,102.15 % and 36.87 % over the base case (without AHT) in power production, cooling and heating effect [26].

AHT coupled with a desalination system is an attractive option for water purification using low-temperature waste heat [27]. Saren et al. [28] proposed a novel configuration of AHT driven MED system. The system uses a low-grade heat at 59^{o}C and upgrades it with the help of AHT. Further, the upgraded heat is used to heat the feed water and produce the distillate in the MED system. A simulation model has been developed to predict the performance characteristics such as

coefficient of performance (COP), distilled water output, total specific thermal energy consumption (TSTEC) and performance ratio (PR) of the coupled system for various water-based working fluid combinations. For waste heat input in the temperature range of 60ºC to 80ºC and sink temperature in the range of 20ºC to 40ºC, the performance of the system is compared, while considering gross temperature lift (GTL) up to 40ºC [29]. Salata and Coppi [30] demonstrated a solar pond driven AHT system, whose heat is used for desalination purposes. A lab scale pilot unit of AHT driven distillate system produced distillate flow at 4.1 L/hr at absorber temperature of 100ºC with a COP and temperature lift of 0.3 – 0.38 and 20ºC [31]. Romero and Martinez [32] used waste heat in the temperature range of 60-80ºC to generate absorber temperature of 100ºC and further providing distillate. Colorado et al. [33] performed a detailed exergy analysis and reported that the highest irreversibility occurs in desorber and absorber. They used single effect evaporation to produce the distillate. A thermodynamic study with optimization has been used for the maximization of water production rate [34]. Khamooshi et al. [35] presented a novel configuration of double absorption heat transformer where a part of condenser output water is directed to the primary absorber, where it gets heated and further absorbed in the secondary absorber to produce the required amount of heat for desalination. The authors used a single-stage, double stage [36], triple stage [37] and four effect type open absorption heat transformer to produce distillate from waste heat input temperature at 60ºC [38]. The heat of condensation in the auxiliary condenser is further utilized as an input to one of the components, i.e. desorber, evaporator or both. This regeneration heat results in improved COP of the system by 110.3%, 61.5% and 75.3% [39].

Alelyani et al. [40] presented a multi-effect distillation (MED) integrating single and double effect ammonia-water-based VARS. The exhaust heat from the rectifier and the condenser of the VARS system is used to heat the feed water to the top temperature. Further, the second law analysis along with cost analysis for water production and the cooling was performed. The results show that a 2 stage NH_3-H_2O-MED system outperforms the standalone 2-stage cycle with a decrease in the cooling production cost by 42%. Abdulrahim and Darwish [41] proposed a low temperature operated MED system. The Water vapour generated in the desorber of the LiBr-water based absorption system is used as a heat for the MED system. A mathematical model is prepared for the MED, absorption and the solar field. They compared this present hybrid cycle with the standalone LT-MED with the same available heat source. Solar still driven desalination system

also provide an economical method for the production of freshwater. The use of jute covered plastic balls [42], sand filled cotton bag [43] and ultrasonic fogger [44] in conventional solar still have been done to increase the available surface area of heat transfer and increase rate of production of distillate. Ayou et al [45] presented a numerical model polygeneration system with NH_3-H_2O based refrigeration and power cycle integrated with membrane-based desalination. The condenser and absorber heat is used to heat the feedwater for the membrane distillation process. Solar thermal collectors and biogas fired boiler provide the heat to the desorber of the VARS system, and biogas fired boiler. Wang and Lior [46] presented a mathematical model for LiBr-H_2O based VARS integrated MEE desalination plant, run by the exhaust heat from the condenser. The condenser pressure is kept high, which will eventually help obtain the required input temperature for MEE. Mehrpooya et al. [47] used concentrated solar power (CSP) to run the thermal power plant. The exhaust heat from the thermal power plant is used to drive the absorption and desalination systems. They represented the 4632 kW of electrical power, the refrigeration effect of 820.8 kW, and the mass flow rate of distillate produced using the given solar thermal energy to be 22.79 kg/s.

HDH is one of the possible desalination techniques. The significance of the HDH desalination system can be summarized as follows: [4,48]

- Lower cost of operation and maintenance
- Can be used for decentralised production of water.
- Uses low grade of energy and can operate in the lower temperature range.
- Serve as great option when targeting towards zero liquid discharge (ZLD)

For more clarity, a detailed literature review is being presented for the HDH system in Table 2.

Table 2: Summary of HDH desalination systems

System/ Study type	Key outcome	Reference
HDH/Numerical	• An open air open water (OAOW) air heated HDH cycle produced distillate in the range of 17.7-52.1 (kg/hr) with GOR ranging between 1.57-4.7.	Al-Sulaiman et al., 2015 [49]

	• The proposed system work efficiently if operated above the pressure ratio of 0.6 with an effective specific energy consumption of 18.35 kg/kW-hr.	Xu et al., 2019, [50]
	• Water production rate was reported to be 2.89 \$/m^3 for the optimal mass flow rate ratio of 1.3.	Qasem et al., 2020, [51]
	• Single extraction leads to increase in the GOR by 58%.	Chehayeb et al., 2015, [52]
	• For the heat capacity ratio of one, there is minimisation in the entropy generation.	
	• Extraction point location is a vital parameter for the GOR improvement.	
	• The distillate production rate was increased by 50 %, when the humidifier pressure was reduced from 1.1 to 0.9 bar.	Rahimi-Ahar et al., 2018a , [53]
	• The atmospheric dehumidifier GOR was 139.13 % higher than the over-atmospheric dehumidifier one.	
	• Desiccant wheel was used to increase the temperature and reduction in the moisture content of the air before inlet to the humidifier.	S.A. et al., 2018 [54]
	• The system with the desiccant wheel shows prominent results over conventional HDH system in terms of increased GOR.	
HDH/Experimental	• The experimental analysis shows a maximum increased humidity ratio of 0.187 kg w.v/ kg air was reported with 20.6 L/m^2 of distillate production rate.	Srithar and Rajaseenivasan, 2017, [55]
	• The increased mass flow rate of air leads to improvement in the humidifier performance.	
	• Tabulators can be used to improve the distillate production rate.	
	• The water production rate was reported as low as 3.86 \$/ton for a multistage HDH system	Zhao et al., 2019, [56]
	• An improvement in GOR and $\dot{M}d$ was reported for reduction in the operating pressure from 90 kPa to 50 kPa for a vacuum operated HDH system.	Rahimi-Ahar et al., 2018b , [57]
	• Response surface methodology can be implemented for achieving the optimum operating parameters.	
	• A day round water production can be achieved with the help of geothermal energy.	Elminshawy et al., 2016, [58]
	• The distillate production rate and the GOR of the system increases with an increase in the top temperature.	

	• Dehumidifier effectiveness has a greater effect over humidifier effectiveness, for the system performance. • Utilisation of brine heat improved the ssyem performance by 100%, compared to OAOW configuration.	Zubair et al., 2018, [59]
HDH/VCR	• The condenser of the VCR is used to preheat the feedwater and the required heating is done with the help of a solar water heater (SWH) to raise the temperature of the feed water to the required top temperature. • the evaporator of the VCR cycle is used to provide the required cooling and also act as dehumidifier to condense the vapour from the air at the outlet of the humidifier	Tangellapalli, 2021, [60]
	• The condition of the supply air was in the range of 30-50 ºC and 0. • 02-0.05 kg. of w.v/kg of d.a • The total saving in the operating cost decreases with an increase in the outdoor air flow rate for any given temperature. • The maximum saving was reported to be 1079 $/year.	Fouda et al., 2016, [61]
	• Distillate production rate and the cooling capacity increases with an increase in the outdoor air temperature. • For heating system, a reduced temperature and flow rate leads to higher COP of the system.	Elattar et al., 2016, [62]
HDH/VARS	• a hybrid solar biomass system that provided cooling and desalination through LiBr driven VARS and HDH desalination systems • The condenser's heat drives the HDH system at a top temperature of 81ºC	Sahoo et al., 2017, [63]
	• The two stage HDH system which was driven by heat from the solar water heater (flat plate heater) and the ammonia-water based VARS cycle is operated from the heat supplied by the scheffler reflector operated solar water heater. The air outlet at the second dehumidifier is further cooled with the help of the chilled water from the VARS system and further this chilled air is supplied to the desired room	Chiranjeevi and Srinivas, 2014, [64]
	• Humidified air, chilled water temperature and volume fraction are vital parameters for the systems performance. • 2.2 L/h of distillate is produced for 100L/h of feed water.	Marale et al., 2017, [65]

- The conditioned air was supplied at 21 ºC and 67 % Rh.

According to the literature survey, it is clear that a combination of absorption heat transformer (AHT), vapour absorption refrigeration system (VARS) and humidification-dehumidification (HDH) system has been never proposed earlier. The AHT increases the grade of waste heat which is available at 70-90ºC and this upgraded heat is used to drive a coupled VARS-HDH system. This paper presents a novel combination of an absorption heat transformer (AHT), a vapour absorption refrigeration system (VARS) and a humidification-dehumidification (HDH) desalination system. This system will not only provide refrigeration (between −5ºC to −15ºC) with the help of waste heat at temperature of 90ºC, which will be helpful in the storage of highly perishable medicine and frozen food stuff, but will also provide freshwater. The mathematical model is prepared for the proposed system and solved with the help of MATLAB. Further the second law analysis (exergy analysis) is also performed. The temperature dependence is analysed by calculating the performance parameters such as coefficient of performance, gain output ratio and refrigeration effect of the system is evaluated at different evaporator and desorber temperatures.

2. AHT-driven combined VARS and HDH unit

The schematic of the AHT-driven combined VARS and HDH unit is shown in Fig. 1. As seen in the figure, the proposed cycle consists of three main components, i.e. an absorption heat transformer (AHT), a vapour absorption refrigeration (VAR) system, and a humidification-dehumidification (HDH) desalination system.

The first system of the proposed cycle is AHT, where the grade of waste-heat is increased by increasing its temperature. It consists of a desorber, condenser, evaporator, absorber and a solution pump. Generally, the operating temperature of the evaporator and the desorber is the same and is operated by a common waste heat source. The absorber of AHT supplies the upgraded heat. The present study comprises of LiBr-H_2O driven AHT system, with LiBr as absorbent and H_2O as a refrigerant. In LiBr-H_2O pair, the solution rich in absorbent is termed as a strong solution. The liquid refrigerant entering the evaporator#1 is heated by waste heat to change the phase of the refrigerant to vapour. At state-2, the refrigerant vapour coming out of the evaporator gets absorbed

in the strong solution (state-8) in absorber#1, leading to the release of the absorption heat. Further, the generated heat is transferred from the system with the help of an external loop (process 7-8). The weak solution of absorber#1 (state-3) is then transferred to the desorber. Before the desorber, the weak solution releases its heat to the strong solution in the sensible heat exchanger (SHX) (process 3-4), and then this solution is expanded (process 4-5) to a lower pressure of the system with the help of throttling device. Waste heat is supplied in the desorber to remove the absorbed refrigerant and then the strong solution obtained (state-6) is again pumped to the absorber#1. The refrigerant vapour (state-9), is then cooled in the condenser, and the cooled refrigerant (state-10) is then pumped to a higher pressure at the inlet of the evaporator (state-1). The AHT works at two pressure levels; the evaporator and the absorber operate at a higher pressure, and the condenser and desorber operate at lower pressure. Contrary to this, in VARS the evaporator and absorber work at lower pressure and the desorber and condenser works at higher pressure.

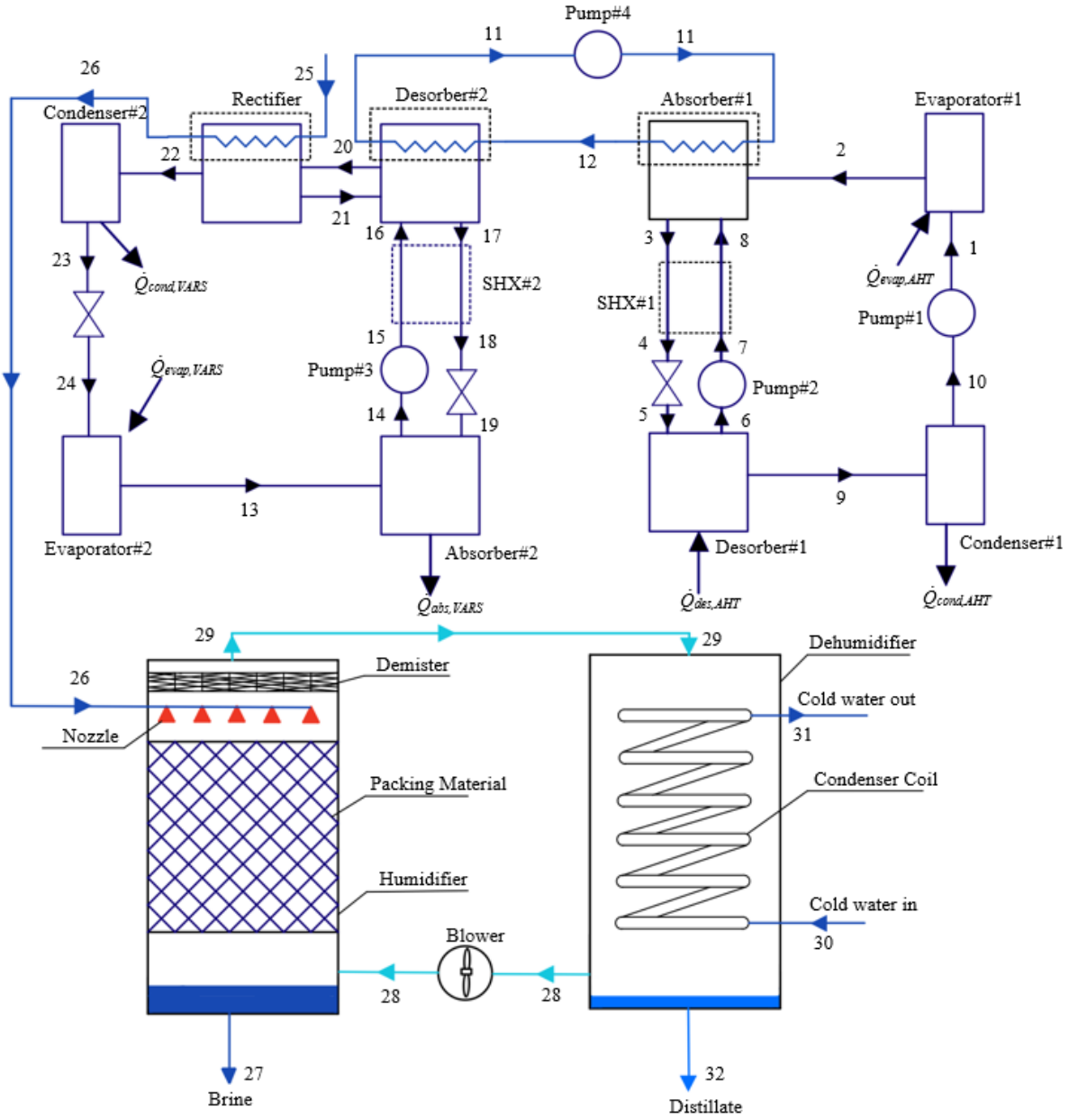

Fig. 1 Schematic of the proposed novel cycle consisting of an absorber heat transformer, vapour absorption refrigeration system and a humidification-dehumidification system.

The second system is vapour absorption refrigeration system (VARS). The VARS consist of NH_3-H_2O as a working pair, with ammonia as a refrigerant and water as absorbent. Refrigerant vapour at state-13 get mixed with the solution (state-19) in the absorber#2, and the heat of absorption is thrown away to the ambient ($\dot{Q}_{abs,\mathrm{VARS}}$). The strong solution (state-14) of ammonia

and water (here in VARS strong solution means, the solution rich in refrigerant) is pumped to the state-15, after which it is passed through the SHX, where it gets heated to state-16, by exchanging heat with the weak solution coming out from the absorber#2. Waste heat required to separate the refrigerant from the solution in the desorber#2 is supplied from the heat of absorption released from the absorber#1 of AHT via loop 12-11. The remaining weak solution (state-17) is again sent back to absorber#2. The generated vapour (state-20) contains traces of absorbent (water), so to remove the absorbent from the refrigerant, the vapour is passed through the rectifier, and nearly pure refrigerant is produced at the outlet of the rectifier (state-22). The removed absorbent is again fed to the desorber through the state-21. The refrigerant phase change occurs in condenser#2, and liquid refrigerant is obtained at its outlet (state-23). The refrigerant is further expanded to lower pressure (state-24) through the throttling device, and the reduced temperature refrigerant provides the required refrigeration in the evaporator (process 24-13).

The third system is the HDH desalination. Heated water (state-26) is sprayed from the top of the humidifier, with the help of spraying nozzles. The middle section of the humidifier is filled with packing material, so that the effectiveness of the humidifier can be improved. Packing material is used in the humidifier to increase the surface area and the time of water contact with the air. Air is supplied from the bottom of the humidifier (state-28). The supplied air at the outlet of the humidifier gets heated and humidified while interacting with the heated water in the packing material section. The air at state-29 (humidifier outlet) is heated and humidified and supplied to the dehumidifier. In a dehumidifier, the air gets cooled while interacting with the cold feedwater flowing (process 30-31) in the condenser coil. The condensed water at the bottom of the dehumidifier (state-32) is collected and is our required distillate. The configuration of the HDH system used here is closed air open water type, and the blower is used for the flow of air.

In the current proposed system, the absorber#1 heat is used as a heat source for the desorber#2 of the VAR system. The feed water takes the rectifier heat (state-25) and is used to heat the feed water source (state-26) to the desired top temperature.

3. Mathematical Modelling of the System

The mathematical model for the present system consists of the individual models for each unit which will be explained in the subsection below.

The modeling of the proposed system is performed considering the following assumptions [66,67]

- Steady-state analysis.
- Pump and blower power were neglected, as their power consumption is minimal compared to other components of the system.
- Kinetic and potential energy neglected.
- No leakage from the system.
- States 3, 6, 10, 14, 17 and 23 are saturated liquid.
- States 2 and 13 are saturated vapour.
- Pressure drops across pipes are neglected.

3.1 Absorption heat transformer (AHT)

The input parameters for AHT are evaporator and condenser temperature. For calculation of amount of temperature lift that can be obtained in the AHT, we have to calculate solution dew point temperature in the absorber and the generator. The solution dew point temperature and the enthalpy of the solution can be found with the given empirical relations in terms of solution temperature and mass fraction. The values of the coefficients can be taken from Sun 1997 [68].

$$T_d = \sum_{i=0}^{5} \sum_{j=o}^{2} a_{ij} \, X^i \, T^j \tag{1}$$

$$h = \sum_{i=0}^{5} \sum_{j=o}^{2} b_{ij} \, X^i \, T^j \tag{2}$$

The input variable includes the evaporator, absorber, condenser, and desorber temperature. Also, the solution flow rate from the desorber to the absorber is also taken as the input value. For a given desorber temperature, the extra refrigerant is removed from the solution in the desorber to make the mass fraction of the solution in accordance with the saturation mass fraction. After the calculation of the properties at various state points in the system, the heat transfer across various sub-components can be calculated.

$$\dot{Q}_{cond,AHT} = \dot{m}_9(h_9 - h_{10}) \tag{3}$$

$$\dot{Q}_{abs,AHT} = \dot{m}_2 h_2 + \dot{m}_8 h_8 - \dot{m}_3 h_3 \tag{4}$$

$$\dot{Q}_{des,AHT} = \dot{m}_6 h_6 + \dot{m}_9 h_9 - \dot{m}_5 h_5 \tag{5}$$

$$\dot{Q}_{evap,AHT} = \dot{m}_1(h_2 - h_1) \tag{6}$$

The COP of the AHT can be calculated as [68].

$$COP_{AHT} = \frac{\dot{Q}_{abs,AHT}}{\dot{Q}_{des,AHT} + \dot{Q}_{evap,AHT}} \tag{7}$$

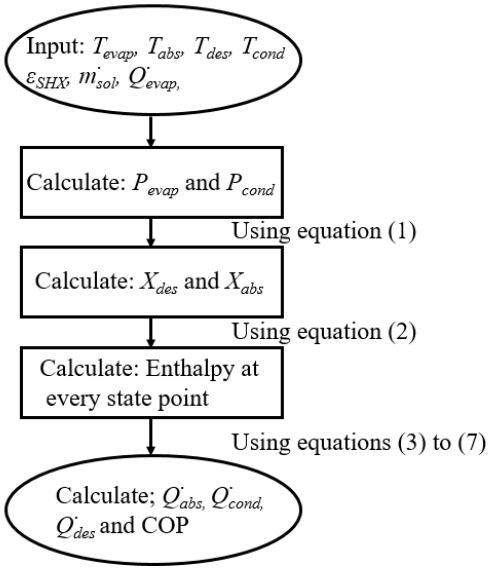

Fig. 2 Algorithm to design the AHT.

3.2 Vapour absorption refrigeration system (VARS)

The amount of refrigerant absorbed in the absorber and the amount of refrigerant removed from the absorber-absorbent solution in the desorber can be calculated from the temperature which is maintained in the absorber and the desorber of the vapour absorption refrigeration system. The state point temperature and enthalpy are the function of the corresponding pressure, temperature and mass fraction [69].

$$T = T_o \sum_i a_i (1-x)^{k_i} \left[ln\left(\frac{p_o}{p}\right)\right]^{n_i} \tag{8}$$

$$h_L = h_o \sum_i a_i \left(\frac{T}{T_o} - 1\right)^{k_i} x^{n_i} \tag{9}$$

$$h_G = h_o \sum_i a_i \left(1 - \frac{T}{T_o}\right)^{k_i} (1-y)^{\frac{n_i}{4}} \tag{10}$$

The coefficient of the above equations can be taken from the Patek and Klomfar [69]. The reference temperature, reference pressure, and the reference enthalpy are 273.16K, 2MP and 100kJ/kg.

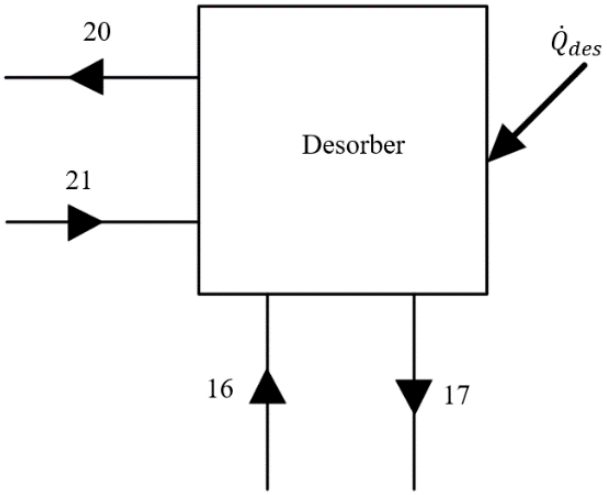

Fig. 3 Schematic of heat and fluid flow interactions in desorber of VARS.

To calculate the mass flow rate of the refrigerant through the VARS, the energy and mass balance is applied across the desorber (Fig. 3),

$$\dot{m}_{16} = \dot{m}_{17} + \dot{m}_{20} - \dot{m}_{21} \tag{11}$$

$$\dot{m}_{16}X_{16} = \dot{m}_{17}X_{17} + \dot{m}_{20}Y_{20} - \dot{m}_{21}X_{21} \tag{12}$$

All the unknown mass flow rates are calculated using the above two equations. Now various heat transfers across the sub-component of the VARS are calculated, which are described below

$$\dot{Q}_{cond,VARS} = \dot{m}_9(h_9 - h_{10}) \tag{13}$$

$$\dot{Q}_{abs,VARS} = \dot{m}_2 h_2 + \dot{m}_8 h_8 - \dot{m}_3 h_3 \tag{14}$$

$$\dot{Q}_{des,VARS} = \dot{m}_6 h_6 + \dot{m}_9 h_9 - \dot{m}_5 h_5 \tag{15}$$

$$\dot{Q}_{evap,VARS} = \dot{m}_{13}(h_{13} - h_{24}) \tag{16}$$

The COP of the VARS can be calculated as [70]

$$COP = \frac{\dot{Q}_{evap,VARS}}{\dot{Q}_{des,VARS}} \tag{17}$$

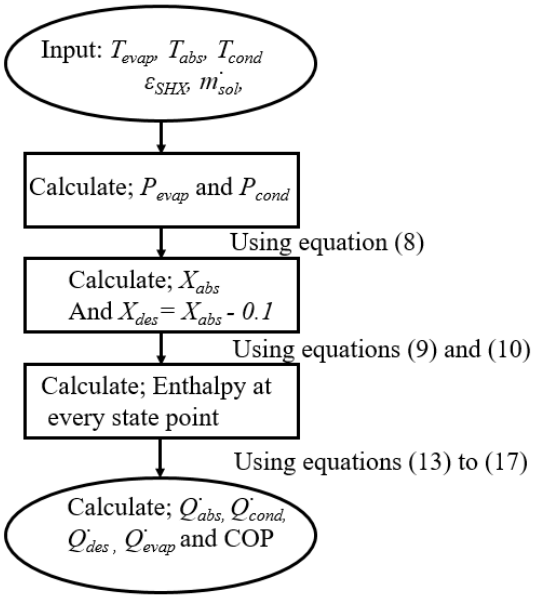

Fig. 4 Algorithm to design the VARS.

3.3 Humidification-dehumidification (HDH) desalination system

The one of the important parameter for the modelling of the HDH desalination system is its effectiveness, which is the ratio of the actual enthalpy change rate to the maximum change [71]

$$\varepsilon = \frac{\Delta \dot{H}}{\Delta \dot{H}_{max}} \tag{18}$$

The maximum enthalpy change rate of water and water can be calculated by the equation

$$\Delta \dot{H}_{max,a} = \dot{m}_a \left(h_{a,H,o,ideal} - h_{a,H,i} \right) \tag{19}$$

$$\Delta \dot{H}_{max,w} = \dot{m}_w \left(h_{w,H,i} - h_{w,H,o,ideal} \right) \tag{20}$$

where $h_{a,H,o,ideal}$ is calculated at the inlet water temperature to humidifier and similarly $h_{w,H,o,ideal}$ is calculated at inlet air temperature to humidifier.

if;

$$\Delta \dot{H}_{max,w} > \Delta \dot{H}_{max,a} \tag{21}$$

$$\varepsilon_H = \left(\frac{h_{w,H,i} - h_{w,H,o}}{h_{w,H,i} - h_{w,H,o,ideal}} \right) \tag{22}$$

Otherwise if;

$$\Delta \dot{H}_{max,w} < \Delta \dot{H}_{max,a} \tag{23}$$

$$\varepsilon_H = \left(\frac{h_{a,H,o} - h_{a,H,i}}{h_{a,H,o,ideal} - h_{a,H,i}}\right) \quad (24)$$

To calculate the remaining parameters of the humidifier, the energy balance is applied through the control volume of the humidifier;

$$\dot{m}_w\left(h_{w,H,i} - h_{w,H,o}\right) = \dot{m}_a\left(h_{a,H,o} - h_{a,H,i}\right) \quad (25)$$

Similar to this, the modelling of the dehumidifier can be performed.

$$h_{a,DH,i} = h_{a,H,o} \quad (26)$$

$$\Delta\dot{H}_{max,a} = \dot{m}_a\left(h_{a,DH,i} - h_{a,DH,o,ideal}\right) \quad (27)$$

$$\Delta\dot{H}_{max,w} = \dot{m}_w\left(h_{w,DH,o,ideal} - h_{w,DH,i}\right) \quad (28)$$

Where $h_{a,DH,o,ideal}$ is calculated at the inlet water temperature to dehumidifier and similarly $h_{w,H,o,ideal}$ is calculated at inlet air temperature to dehumidifier.

if;

$$\Delta\dot{H}_{max,w} > \Delta\dot{H}_{max,a} \quad (29)$$

$$\varepsilon_{DH} = \left(\frac{h_{w,DH,o} - h_{w,DH,i}}{h_{w,DH,o,ideal} - h_{w,DH,i}}\right) \quad (30)$$

Otherwise if;

$$\Delta\dot{H}_{max,w} < \Delta\dot{H}_{max,a} \quad (31)$$

$$\varepsilon_{DH} = \left(\frac{h_{a,DH,i} - h_{a,DHo}}{h_{w,DH,i} - h_{w,DH,o,ideal}}\right) \quad (32)$$

To calculate the remaining parameters of the dehumidifier, the energy balance is applied through the control volume of the dehumidifier;

$$\dot{m}_w\left(h_{w,DH,o} - h_{w,DH,i}\right) + \dot{m}_d h_d = \dot{m}_a\left(h_{a,DH,i} - h_{a,DH,o}\right) \quad (33)$$

The mass flow rate of distillate produced can be calculated as

$$\dot{m}_d = \dot{m}_a\left(\omega_{H,o} - \omega_{H,i}\right) \quad (34)$$

The heat input to the HDH system can be calculated as:

$$\dot{Q} = \dot{m}_w\left(h_{w,H,i} - h_{w,f}\right) \quad (35)$$

The performance parameter, i.e. the GOR for the HDH system can be measured as [71]

$$GOR = \frac{\dot{m}_d h_{fg}}{\dot{Q}} \quad (36)$$

The governing equations for AHT, VARS and HDH system are then solved numerically using MATLAB software. Further a detailed modelling of HDH system can be referred from Beniwal et al. [48].

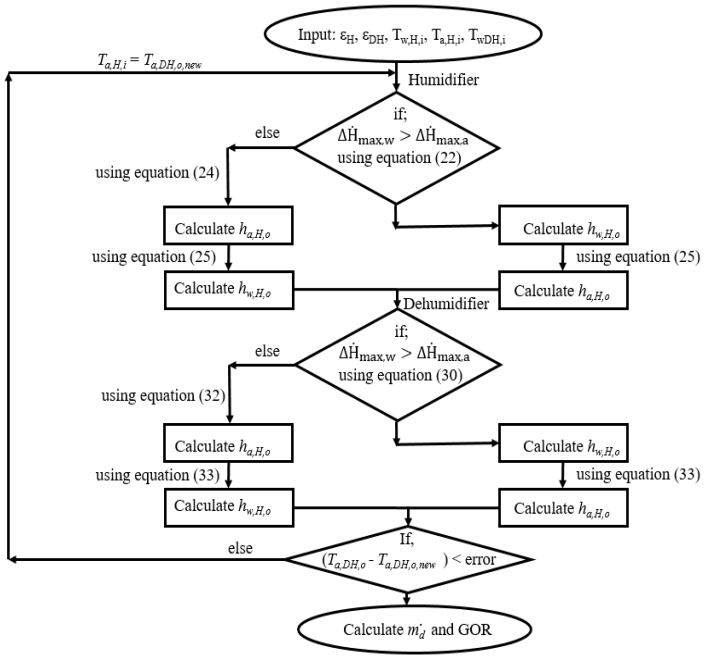

Fig. 5 Algorithm to design the HDH desalination system.

3.4 Exergy analysis

The term Exergy refers to the maximum amount of work that can be extracted from a system when it is allowed to come in the equilibrium to the environment. It composed of four main components [72] i.e.

$$E = E^{PH} + E^{CH} + E^{PT} + E^{KN} \tag{37}$$

Where E^{PH} refers to physical exergy, E^{CH} refers to chemical exergy, E^{PT} refers to potential exergy and E^{KN} refers to kinetic exergy.

Following are the assumptions made during the exergy analysis of the system [73]

- The chemical, potential and kinetic exergies are neglected
- The analysis is performed under steady state operations of the individual components
- The reference temperature is assumed to be 25°C and reference pressure to be 1 bar.

- Exergy destruction across solution pump is neglected due to its very minimal power consumption compared to other components of the system. Therefore the exergy associated with the pump will be of negligible order compared to that of the system.

Under steady state, the rate of exergy destruction can be calculates as [72]

$$\dot{E}_D = \dot{Q}\left(1 - \frac{T_o}{T}\right) + \dot{E}_{in} - \dot{E}_{out} - \dot{W} \tag{38}$$

Where $\dot{E}$ refers to the flow exergy and is calculated at every state point specified. It can be calculated as [72]

$$\dot{E} = \dot{m}(h - h_o) - T_o(s - s_o) \tag{39}$$

Table 3: Exergy relations for various components of the system.

Components	Exergy relations
Evaporator#1	$\dot{E}_{D,evap,AHT} = \dot{Q}_{evap,AHT}\left(1 - \frac{T_o}{T_{evap\#1}}\right) + \dot{E}_1 - \dot{E}_2$
Absorber#1	$\dot{E}_{D,abs,AHT} = \dot{E}_2 + \dot{E}_8 + \dot{E}_{11} - \dot{E}_3 - \dot{E}_{12}$
SHX#1	$\dot{E}_{D,SHX\#1} = \dot{E}_3 + \dot{E}_7 - \dot{E}_4 - \dot{E}_8$
Desorber#1	$\dot{E}_{D,des,AHT} = \dot{Q}_{des,AHT}\left(1 - \frac{T_o}{T_{des\#1}}\right) + \dot{E}_5 - \dot{E}_6 - \dot{E}_9$
Pump#2	$\dot{E}_{D,P\#2} = \dot{E}_6 - \dot{W}_{P\#2} - \dot{E}_7$
Condenser#1	$\dot{E}_{D,cond,AHT} = \dot{E}_9 - \dot{Q}_{cond,AHT}\left(1 - \frac{T_o}{T_{cond,AHT}}\right) - \dot{E}_{10}$
Pump#1	$\dot{E}_{D,P\#1} = \dot{E}_{10} - \dot{W}_{P\#2} - \dot{E}_1$
Evaporator#2	$\dot{E}_{D,evap,VARS} = \dot{Q}_{evap,VARS}\left(1 - \frac{T_o}{T_{evap,VARS}}\right) + \dot{E}_{24} - \dot{E}_{13}$
Absorber#2	$\dot{E}_{D,abs,VARS} = \dot{E}_{13} + \dot{E}_{19} - \dot{E}_{14} - \dot{Q}_{abs,VARS}\left(1 - \frac{T_o}{T_{abs,VARS}}\right)$
Pump#3	$\dot{E}_{D,P\#1} = \dot{E}_{14} - \dot{W}_{P\#3} - \dot{E}_{15}$
SHX#2	$\dot{E}_{D,SHX\#2} = \dot{E}_{15} + \dot{E}_{17} - \dot{E}_{16} - \dot{E}_{18}$
Desorber#2	$\dot{E}_{D,des,VARS} = \dot{E}_{16} + \dot{E}_{21} + \dot{E}_{12} - \dot{E}_{17} - \dot{E}_{20}$
Rectifier	$\dot{E}_{D,rect} = \dot{E}_{20} + \dot{E}_{25} - \dot{E}_{21} - \dot{E}_{22} - \dot{E}_{26}$
Condenser#2	$\dot{E}_{D,cond,VARS} = \dot{E}_{22} - \dot{Q}_{cond,VARS}\left(1 - \frac{T_o}{T_{cond,VARS}}\right) - \dot{E}_{23}$

Humidifier	$\dot{E}_{D,H} = \dot{E}_{26} + \dot{E}_{28} - \dot{E}_{27} - \dot{E}_{29}$
Dehumidifier	$\dot{E}_{D,DH} = \dot{E}_{29} + \dot{E}_{30} - \dot{E}_{28} - \dot{E}_{31} - \dot{E}_{32}$

4. Results and Discussion

The mathematical equations presented in section 3 are then solved mathematically using the simulation program MATLAB. The simulated results of the individual systems are then validated with the published data, as shown in section 4.1. The variation in COP of AHT and VARS is also analyzed for their different operating values of evaporator and desorber temperature. The rectifier heat is used to heat the feed water to achieve the required top temperature. The top temperature is varied by varying the feed flow rate through the rectifier. The mass flow rate of distillate ($\dot{M}_d$) produced for the HDH system is also analyzed for different mass flow rate ratios ($\dot{M}_r$) and varied top temperatures. Table 4 shows the values used for the numerical study of the proposed system. As for VARS system, we want to transfer the latent heat of phase change in the condenser, and the heat of absorption for the absorber to the ambient; therefore for corresponding to the ambient conditions, we are keeping the similar values for the absorber and condenser.

Table 4: Input values for thermodynamic study of the proposed system

Input Parameter	Value
$\dot{m}_{sol,AHT}$	1 kg/sec
$\dot{Q}_{evap,AHT}$	300 kW
$T_{cond,AHT}$	35 ºC
$\dot{m}_{sol,VARS}$	1 kg/sec
$T_{abs,VARS}$	35 ºC
$T_{cond,VARS}$	35 ºC
$\dot{M}w$	1 kg/sec
$T_{w,DH,i}$	25 ºC
T_f	25 ºC
ε_H	0.80
ε_{DH}	0.80

4.1 Validation of the model

Since the combination of AHT, VARS and HDH desalination systems has not been reported in the literature, individual components validation has been performed. The governing equations are solved using numeric computing program- MATLAB. The validations for the AHT, VARS and HDH desalination system have been performed against numerical model results from other studies.

Thermodynamics analysis of AHT is performed and the parameters used are shown in Table 5. The component performance is evaluated and is compared with the data from the published literature as shown in Table 6. The model (AHT) results are in close agreement with the published data with a maximum variation of 0.7%. Also a COP of 0.48 was reported experimentally for similar operating conditions, with maximum percentage difference of 3% with the numerical model [74].

Table 5: Input values for validation of the AHT cycle [70].

Input Parameter	Value
$T_{evap,AHT}$	101.09 ºC
$T_{abs,AHT}$	153.90 ºC
$T_{des,AHT}$	111.60 ºC
$T_{cond,AHT}$	55.02 ºC
$\dot{Q}_{evap,AHT}$	187.30 kW
$\dot{m}_{sol}$	1.00 kg/sec

Table 6: Validation between the current AHT model and the published data.

Input Parameter	Herold et. al. [70]	Current model	% Difference/Tolerance
$\dot{Q}_{abs,AHT}$ (kW)	184.40	184.12	0.1
$\dot{Q}_{cond,AHT}$ (kW)	188.30	189.61	0.7
$\dot{Q}_{des,AHT}$ (kW)	185.40	185.01	0.2
COP	0.495	0.494	0.2

Similarly, thermodynamics analysis of VARS is performed and the parameters used are shown in Table 7. The component performance is evaluated and is compared with the data from

the published literature as shown in Table 8. The model (VARS) results are in close agreement with the published data, with a maximum variation of 7.63. Also an error of 8% is being reported for the experimental and numerical study for cooling capacity calculations and for the operating conditions of the present study the experimental COP is in range of 0.3 to 0.35 [75].

Table 7: Input values for validation of VARS [70].

Input Parameter	Value
$T_{evap,VARS}$	-10.00 ºC
$T_{abs,VARS}$	40.00 ºC
$T_{des,VARS}$	124.20 ºC
$T_{cond,VARS}$	40.00 ºC
$\dot{m}_{sol}$	1.00 kg/sec

Table 8: Validation between the current VARS model and the published data.

Input Parameter	Herold et. al. [70]	Current model	% Difference/Tolerance
$\dot{Q}_{cond,VARS}$ (kW)	159.20	167.41	5.15
$\dot{Q}_{evap,VARS}$ (kW)	146.90	155.46	5.82
$\dot{Q}_{abs,VARS}$ (kW)	273.90	292.95	6.95
$\dot{Q}_{des,VARS}$ (kW)	327.50	352.52	7.63
$\dot{Q}_{rect,VARS}$ (kW)	42.80	45.13	5.44
COP	0.447	0.441	1.34

The numerical model for the closed air open water (CAOW) HDH system is prepared and is validated against a numerical study performed by Narayan et al. [76].

Table 9: Input values for validation of HDH system.

Input Parameter	Value
$T_{w,H,i}$	80 ºC
$T_{w,DH,i}$	30 ºC
ε_{DH}	0.80

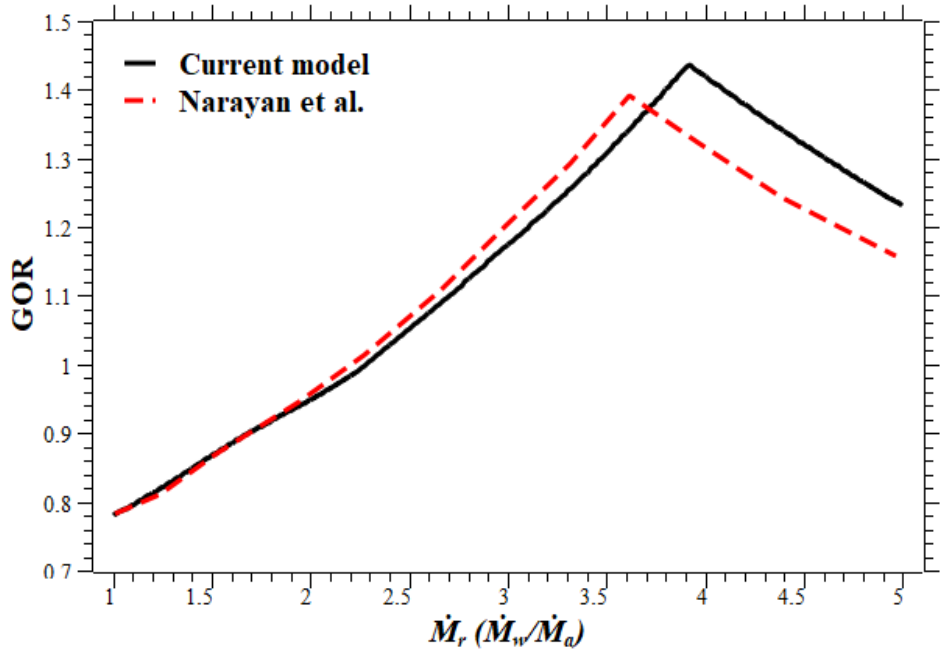

Fig. 6 Variation of GOR of a HDH desalination system with respect to mass flow rate ratio ($\dot{M}_r$) for the present study and validating with Narayan et al. [76]

The mathematical model for the HDH desalination system has been prepared and is validated with the available similar published results by Narayan et al.[76]. Fig 6 shows the validation study, which is the variation of GOR with mass flow rate ratio for the top temperature of 80ºC. As can be seen from Fig. 6, the current HDH desalination model is in close agreement with the result from Narayan et al.[76], with a maximum deviation of 3.08%. When comparing with the experimental system, a GOR of 0.9 has been reported for similar operating conditions [77].

4.2 Variation in COP of the VARS system

Figure 7 shows the variation of COP of a VARS with respect to desorber temperature for various evaporator temperatures. As can be seen from Fig. 7, as the desorber temperature increases for any given evaporator temperature, the COP of the system rises to a point and after which it becomes nearly constant. This pattern is followed for all the evaporator temperatures. As we increase the desorber temperature, the solution temperature at the inlet to the desorber also

increases. The rate of refrigerant removal rate from the solution in the desorber is less than the amount of heat supplied in the desorber, as the desorber temperature increases leading to decrease in the amount of refrigeration corresponding to the heat input and eventually a constant or decrease in the COP value after the maximum point.

Also, as the temperature of the evaporator increases, the maximum value of the COP increases and follows a similar trend as in the case of lower temperature. The increase in the evaporator temperature leads to an increased saturation pressure of the absorber, leading to higher absorption rate of the refrigerant in the absorber. The increase in COP is due to the higher absorption of refrigerant in the absorber due to increased absorber pressure, which means a higher refrigeration effect for the same desorber heat input.

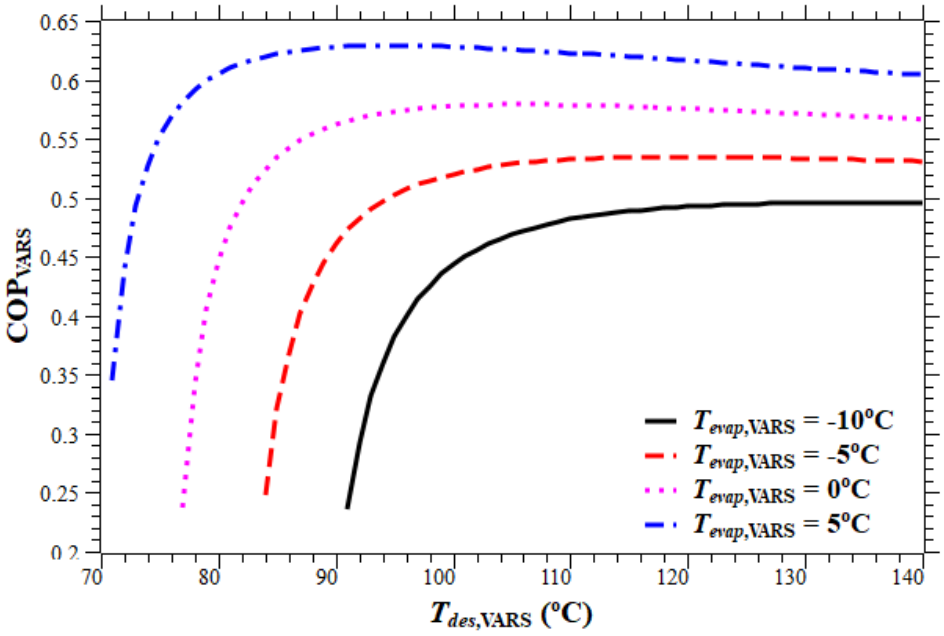

Fig. 7 Variation of COP of a VARS system with respect to desorber temperature for various values of evaporator temperature.

4.3 Variation in COP of the absorber heat transformer

As shown in Fig. 8, by increasing the temperature lift for a given evaporator temperature, the COP of the heat transformer decreases. This happens because as the lift increases so the temperature of the absorber. With an increase in the absorber temperature for a given pressure, the absorption capacity of the solution towards refrigeration decreases, which leads to lesser heat of

absorption. Also, when the evaporator temperature increases, so does the pressure of the evaporator and the absorber. The increased pressure of the absorber tends to increase the absorption capacity of the absorber, and hence higher would be the value of heat of absorption. Due to this reason, the COP of the heat transformer increases with the increase in the evaporator temperature, for a given lift.

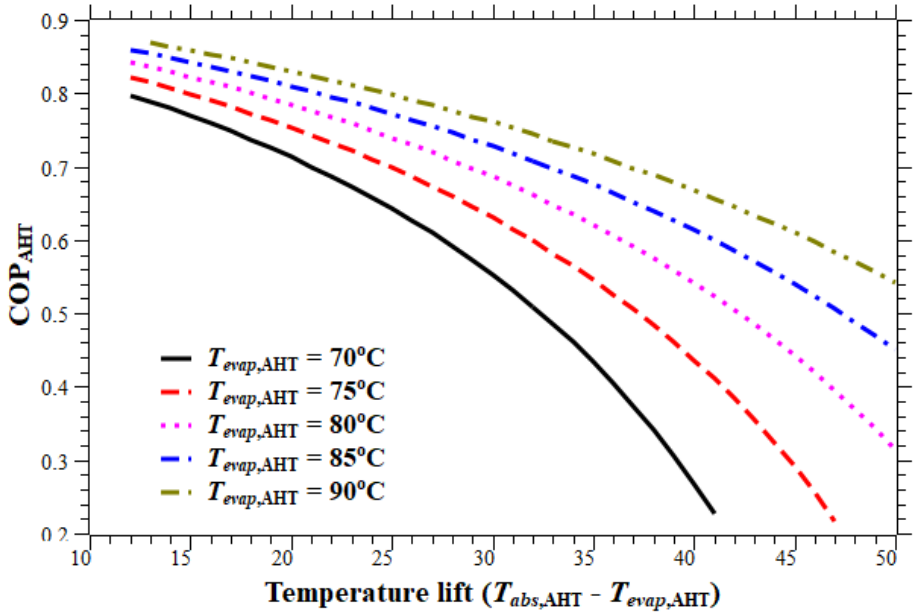

Fig. 8 Variation in COP of an AHT with temperature lifts for various evaporator temperature.

4.4 Variation in the mass flow rate of distillate ($\dot{M}_d$) of the CAOW-HDH desalination cycle

Fig. 9 shows the distillate production rate for different values of top temperature, with varying mass flow rate ratio ($\dot{M}_r$). For a given temperature of water at the inlet of the humidifier, the distillate production rate increases to a maximum point and after which it starts to decrease, for an increase in the mass flow rate ratio. For a constant mass flow rate of water, therefore, with an increase in the mass flow rate ratio, there is a decrease in air flow rate.

As the mass flow rate of air is decreased so, there will be an increase in the temperature of the air at the outlet of the humidifier. Therefore, the overall effect up to the maximum point is the increase in the distillate production rate. After this point, the air temperature at the humidifier outlet increases, but due to the continuous decrease in the mass flow rate of the air, there will be a

decrease in the water content of the air. Also, we can see from Fig. 9 that the optimal mass flow rate of distillate produced increases as the inlet water temperature in the humidifier increases.

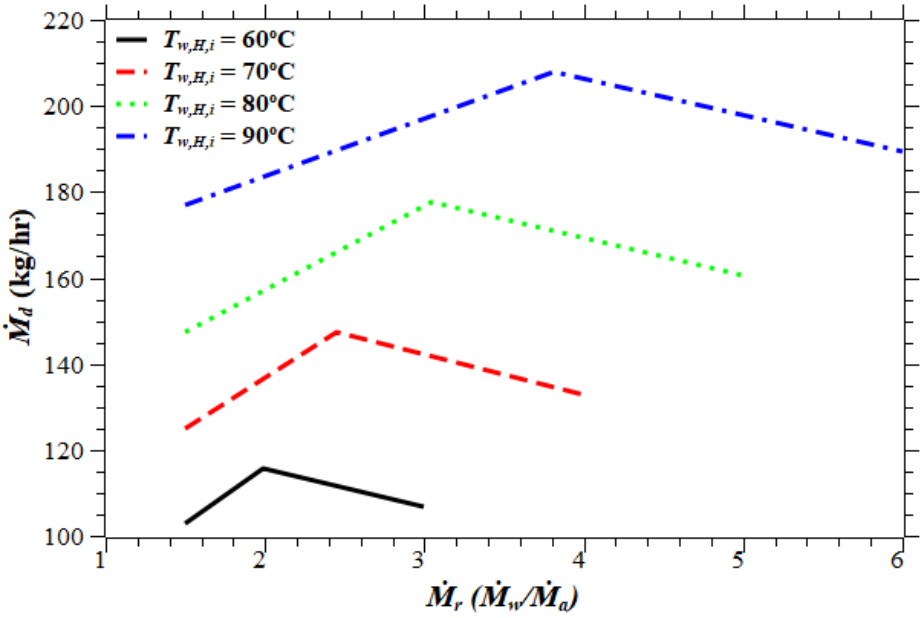

Fig. 9 Effect of top temperature ($T_{w,H,i}$) on distillate production rate ($\dot{M}_d$) for various mass flow rate ratio ($\dot{M}_r$) for single stage humidification-dehumidification desalination (HDH) system.

4.5 Variation in the refrigeration effect of a VARS and mass flow rate of distillate produced

Fig. 10 compares two cases. Initially, 300 kW of waste heat is available at 80°C. If we use this heat directly in a VARS to produce the refrigeration, then below −4°C no refrigeration is possible. This is because the waste heat temperature required to separate the refrigerant out of the solution is less than the saturation temperature of the solution at the inlet of the desorber. As the evaporator temperature increases, so is the absorption of the refrigerant in the absorber (according to Henry law). The higher the concentration of the refrigerant in the solution leads to lowering the solutions' saturation temperature. Therefore nearly after evaporators' temperature of −4°C, the saturation temperature of the solution at the desorber inlet reaches below 80°C, which leads to evaporation of refrigerant in the desorber and eventually, some refrigeration effect is produced.

In the second case when we integrate an AHT system, the waste heat of 300 kW and 80°C is converted to 150 kW of upgraded heat at 110°C. The output heat from the desorber is used as heat input to the VARS. The supply temperature of the heat from the AHT is sufficient enough to produce refrigeration at an evaporator temperature of -14°C and above. As can be seen from figure

10, with the assumed operating conditions (Table 4) the proposed system applicability area is limited to the refrigeration below −2°C, as above which the conventional VARS system will be dominating in providing more amount of refrigeration and the freshwater.

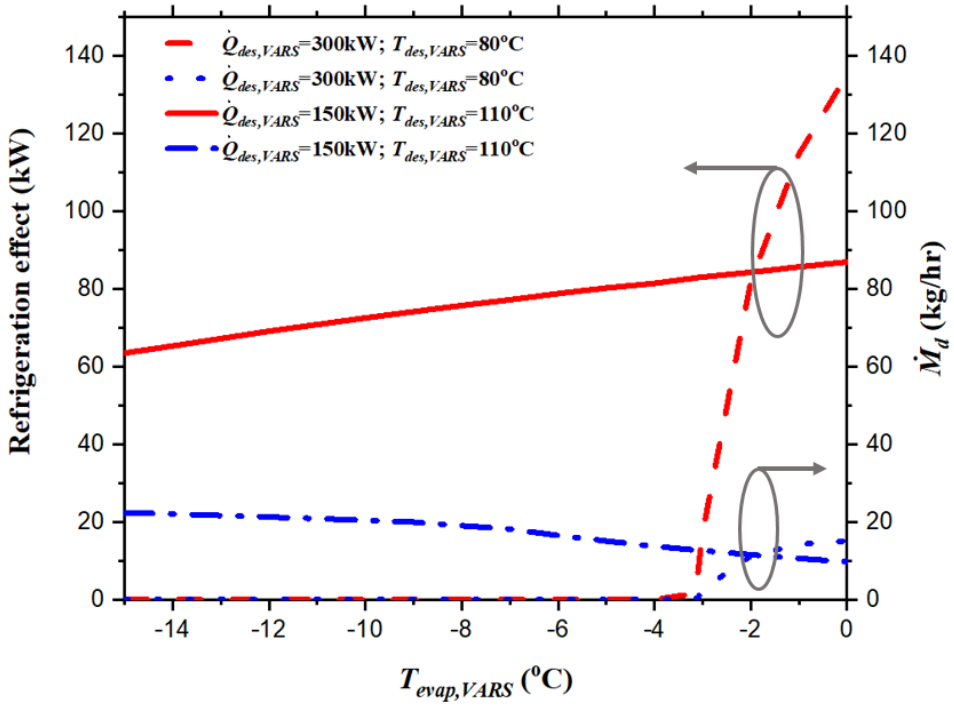

Fig. 10 Effect of Absorption heat transformer on refrigeration effect and distillate production rate for various evaporator temperatures.

4.6 Results of the exergy analysis

To operate the VARS system at the evaporator temperature of -10 °C and condenser temperature of 35 °C, for a cooling effect of 157 kW or 44.65 TR, following are the operating conditions generated for fulfilling the required conditions, as mentioned in the table 10.

Table 10: State point values of operating parameters.

State point	T (°C)	P (kPa)	x (concentration)	$\dot{m}$ (kg/sec)	h (kJ/kg)	s (kJ/kg-K)
1	35.0	47.41	-	0.1884	146.6	8.35
2	80.0	47.41	-	0.1884	2643.0	7.61

3	120.0	47.41	0.55	1.2715	259.5	0.72
4	94.9	47.41	0.55	1.2715	207.3	0.58
5	68.7	5.63	0.55	1.2715	207.3	0.43
6	80.0	5.63	0.60	1.0831	194.2	0.49
7	80.0	47.41	0.60	1.0831	194.4	0.49
8	112.0	47.41	0.60	1.0831	255.7	0.68
9	66.1	5.63	-	0.1884	2629.8	8.53
10	35.0	5.63	-	0.1884	146.6	8.35
11	110.0	200.00	-	16.43	461.4	1.42
12	115.0	200.00	-	16.43	482.6	1.47
13	-10.0	290.64	0.9996	0.1472	1237.9	4.73
14	35.0	290.64	0.42	1	-96.0	0.38
15	35.0	1350.38	0.42	1	-94.7	0.38
16	87.7	1350.38	0.42	1	150.3	1.09
17	112.2	1350.38	0.32	0.8528	290.4	1.41
18	50.4	1350.38	0.32	0.8528	3.2	0.63
19	50.4	290.64	0.32	0.8528	3.2	0.63
20	91.6	1350.38	0.9636	0.1569	1578.8	4.75
21	91.6	1350.38	0.42	0.0097	169.5	1.16
22	39.1	1350.38	0.9996	0.1472	1316.9	4.26
23	35.0	1350.38	0.9996	0.1472	166.3	0.58
24	-10.0	290.64	0.9996	0.1472	166.3	0.65
25	25.0	100.00	-	0.2407	104.8	0.37
26	81.6	100.00	-	0.2407	341.6	1.09
27	49.8	100.00	-	0.2407	208.7	0.70

28	42.7	100.00	-	0.0752	192.0	6.26
29	66.2	100.00	-	0.0752	653.3	7.66
30	25.0	100.00	-	0.2407	104.8	0.37
31	40.0	100.00	-	0.2407	167.6	0.57
32	57.4	100.00	-	0.0122	240.3	0.80

Based on the operating parameters, as mentioned in the Table 10 and the exergy relations as stated in the Table 1, the exergy destruction across various components of the system is presented in the Table 11. As can be seen from the table 11, the maximum exergy destruction in the AHT occurs in the absorber while for VARS, it occurs in the desorber. As the absorber#1 of the AHT and generator#2 of the VARS are at the highest temperature in the corresponding system, therefore the irreversibility attached to it will be maximum for a fixed value of effectiveness of the absorber#1 and generator#2. This leads to the highest exergy destruction among those components of the system, as can be seen from Table 11.

Table 11: Exergy destruction across various components of the system

Components	Exergy destruction (kW)
Evaporator#1	1.91
Absorber#1	15.26
SHX#1	9.0593
Desorber#1	13.18
Condenser#1	0.5846
Evaporator#2	0.91
Absorber#2	11.1716
SHX#2	11.6057
Desorber#2	13.0062
Rectifier	0.3483
Condenser#2	2.3631
Humidifier	0.6233

Dehumidifier	2.6196
Total	82.64

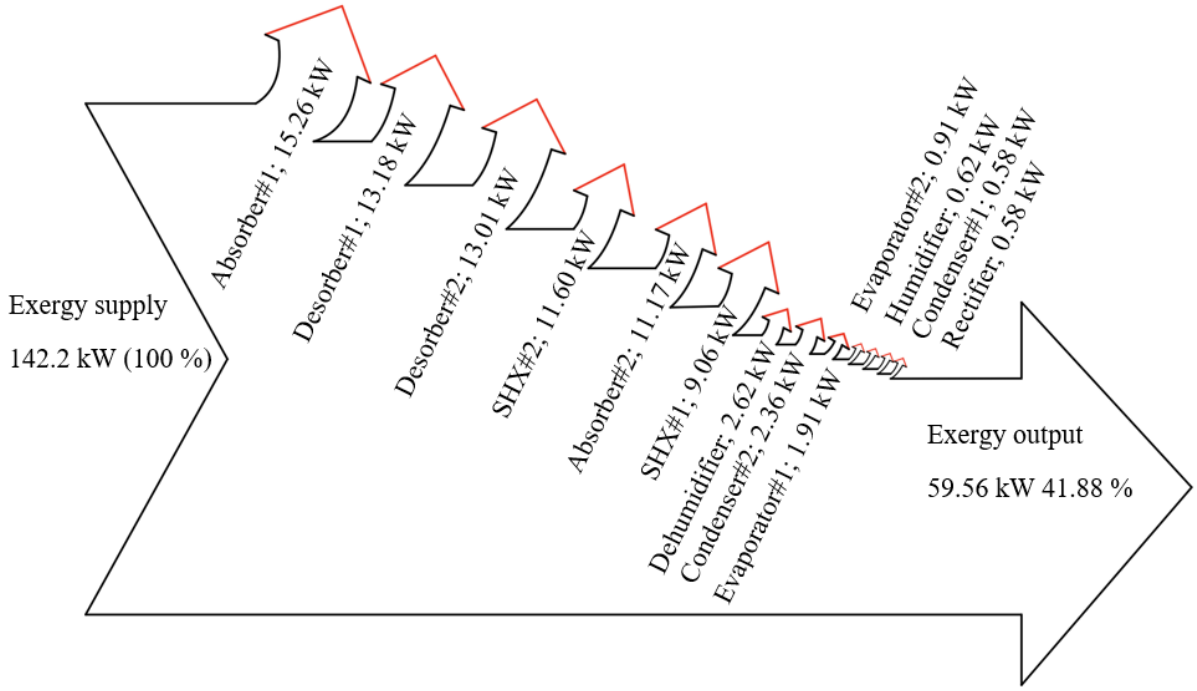

Fig. 11 Grassmann diagram for exergy balance across the proposed system.

5. Conclusion

This paper presented a novel combination of three different technologies i.e. absorption heat transformer (AHT), vapour absorption refrigeration system (VARS) and a humidification-dehumidification (HDH) desalination system. Thermodynamic modeling of the proposed novel system is prepared and solved with the help of MATLAB and thermodynamic performance of the system is predicted in terms of COP, refrigeration temperature and distillate production rate.

- Absorption heat transformer helps in improving the grade of the heat.
- The upgraded heat helps in driving the refrigeration system below the sub-zero temperatures.
- For the assumed systems operating conditions, the AHT helps to operate the VARS below −4°C.

- For 300kW waste heat at 80ºC, for evaporator (VARS) temperature of −10ºC, the system reported 70kW of refrigeration effect is provided with 20kg/hr of distillate production rate.
- Also a total of 84.64 kW of exergy destruction is being reported for an evaporator and condenser temperature of −10ºC and 35ºC.
- Not only the use of AHT helps us to drive the absorption refrigeration systems but also the increased temperature can also be helpful in the process industry such as crop drying, paper mill etc.

For future work, a multistage refrigeration system can be implemented for further utilization of the available energy. Also multistage HDH system can be incorporated to use the heat available of the brine, leaving the humidifier of the single-stage system.

Acknowledgement

The authors wish to acknowledge the support provided by the Department of Mechanical Engineering at Indian Institute of Technology Ropar.

Conflict of Interest

The authors declare no conflict of interest.

CRediT authorship contribution statement

Ravi Beniwal: Writing - original draft, Visualization, Software, Validation. Kapil Garg: Software, Writing - review & editing. Himanshu Tyagi: Writing - review & editing, Supervision.

References

[1] A.H.F. Tsang, W.K. Yung, Development of an Adaptive Food Preservation System for food quality and energy efficiency enhancement, Int. J. Refrig. 76 (2017) 342–355. https://doi.org/10.1016/j.ijrefrig.2017.02.006.

[2] E. Deniz, S. Çınar, Energy, exergy, economic and environmental (4E) analysis of a solar desalination system with humidification-dehumidification, Energy Convers. Manag. 126 (2016) 12–19. https://doi.org/10.1016/j.enconman.2016.07.064.

[3] G.P. Narayan, M.H. Sharqawy, E.K. Summers, J.H. Lienhard, S.M. Zubair, M.A. Antar,

The potential of solar-driven humidification-dehumidification desalination for small-scale decentralized water production, Renew. Sustain. Energy Rev. 14 (2010) 1187–1201. https://doi.org/10.1016/j.rser.2009.11.014.

[4] K. Garg, S.K. Das, H. Tyagi, Thermal design of a humidification-dehumidification desalination cycle consisting of packed-bed humidifier and finned-tube dehumidifier, Int. J. Heat Mass Transf. 183 (2022) 122153. https://doi.org/10.1016/j.ijheatmasstransfer.2021.122153.

[5] C.W. Park, H.C. Cho, Y.T. Kang, The effect of heat transfer additive and surface roughness of micro-scale hatched tubes on absorption performance, Int. J. Refrig. 27 (2004) 264–270. https://doi.org/10.1016/j.ijrefrig.2003.09.008.

[6] D. Triché, S. Bonnot, M. Perier-Muzet, F. Boudéhenn, H. Demasles, N. Caney, Modeling and Experimental Study of an Ammonia-water Falling Film Absorber, Energy Procedia. 91 (2016) 857–867. https://doi.org/10.1016/j.egypro.2016.06.252.

[7] B. Michel, N. Le Pierrès, B. Stutz, Performances of grooved plates falling film absorber, Energy. 138 (2017) 103–117. https://doi.org/10.1016/j.energy.2017.07.026.

[8] L. Yang, K. Du, X.F. Niu, B. Cheng, Y.F. Jiang, Experimental study on enhancement of ammonia-water falling film absorption by adding nano-particles, Int. J. Refrig. 34 (2011) 640–647. https://doi.org/10.1016/j.ijrefrig.2010.12.017.

[9] H. Kim, J. Jeong, Y.T. Kang, Heat and mass transfer enhancement for falling film absorption process by SiO 2 binary nanofluids, Int. J. Refrig. 35 (2012) 645–651. https://doi.org/10.1016/j.ijrefrig.2011.11.018.

[10] S. Wu, C. Rincon Ortiz, Experimental investigation of the effect of magnetic field on vapour absorption with LiBr–H2O nanofluid, Energy. 193 (2020) 1–9. https://doi.org/10.1016/j.energy.2019.116640.

[11] M. Jiang, S. Xu, X. Wu, Experimental investigation for heat and mass transfer characteristics of R124-DMAC bubble absorption in a vertical tubular absorber, Int. J. Heat Mass Transf. 108 (2017) 2198–2210. https://doi.org/10.1016/j.ijheatmasstransfer.2017.01.082.

[12] J. Cerezo, R. Best, J.J. Chan, R.J. Romero, J.I. Hernandez, F. Lara, A theoretical-experimental comparison of an improved ammonia-water bubble absorber by means of a helical static mixer, Energies. 11 (2018) 1–14. https://doi.org/10.3390/en11010056.

[13] J.J. Chan, R. Best, J. Cerezo, M.A. Barrera, F.R. Lezama, Experimental study of a bubble mode absorption with an inner vapor distributor in a plate heat exchanger-type absorber with NH3-LiNO3, Energies. 11 (2018). https://doi.org/10.3390/en11082137.

[14] X. Wu, J. Liu, S. Xu, W. Wang, Effect of vibration parameters on the bubble absorption characteristics of working fluids R134a–DMAC in a vertical tube, Int. J. Refrig. 99 (2019) 234–242. https://doi.org/10.1016/j.ijrefrig.2018.12.024.

[15] W. Wang, S. Xu, X. Wu, M. Jiang, Experimental investigation on heat and mass transfer in a vertical glass bubble absorber with R124-NMP pair, Int. J. Refrig. 112 (2020) 303–313. https://doi.org/10.1016/j.ijrefrig.2019.12.024.

[16] R. Nasr Isfahani, S. Bigham, M. Mortazavi, X. Wei, S. Moghaddam, Impact of micromixing on performance of a membrane-based absorber, Energy. 90 (2015) 997–1004. https://doi.org/10.1016/j.energy.2015.08.006.

[17] S.J. Hong, E. Hihara, C. Dang, Analysis of adiabatic heat and mass transfer of microporous hydrophobic hollow fiber membrane-based generator in vapor absorption refrigeration system, J. Memb. Sci. 564 (2018) 415–427. https://doi.org/10.1016/j.memsci.2018.07.048.

[18] J. He, R. Hirata, E. Hihara, C. Dang, Desorption characteristic of LiBr–H2O solution in hydrophobic hollow fiber membrane for absorption chiller, Appl. Therm. Eng. 195 (2021) 117164. https://doi.org/10.1016/j.applthermaleng.2021.117164.

[19] M. Wang, C. Deng, Y. Wang, X. Feng, Exergoeconomic performance comparison, selection and integration of industrial heat pumps for low grade waste heat recovery, Energy Convers. Manag. 207 (2020) 112532. https://doi.org/10.1016/j.enconman.2020.112532.

[20] B. Liang, M. Chen, Y. Orooji, Effective parameters on the performance of ground heat exchangers: A review of latest advances, Geothermics. 98 (2022) 102283. https://doi.org/10.1016/j.geothermics.2021.102283.

[21] M. Vallès, M. Bourouis, D. Boer, Solar-driven absorption cycle for space heating and cooling, Appl. Therm. Eng. 168 (2020) 114836. https://doi.org/10.1016/j.applthermaleng.2019.114836.

[22] L. Wang, X. Bu, H. Wang, Z. Ma, W. Ma, H. Li, Thermoeconomic evaluation and optimization of LiBr-H2O double absorption heat transformer driven by flat plate

collector, Energy Convers. Manag. 162 (2018) 66–76. https://doi.org/10.1016/j.enconman.2018.02.011.

[23] F. Cudok, N. Giannetti, J.L.C. Ciganda, J. Aoyama, P. Babu, A. Coronas, T. Fujii, N. Inoue, K. Saito, S. Yamaguchi, F. Ziegler, Absorption heat transformer - state-of-the-art of industrial applications, Renew. Sustain. Energy Rev. 141 (2021). https://doi.org/10.1016/j.rser.2021.110757.

[24] S.J. Hong, S.M. Lee, C.H. Lee, I.G. Kim, C.W. Park, Thermally-driven hybrid vapor absorption cycle: Simultaneous and flexible use of steam generation heat pump and refrigeration applications, Energy Convers. Manag. 201 (2019) 112100. https://doi.org/10.1016/j.enconman.2019.112100.

[25] M. Van Der Pal, A. Wemmers, S. Smeding, R. De Boer, Technical and economical feasibility of the hybrid adsorption compression heat pump concept for industrial applications, Appl. Therm. Eng. 61 (2013) 837–840. https://doi.org/10.1016/j.applthermaleng.2013.04.048.

[26] S. Khalilzadeh, A. Hossein Nezhad, A. Romagnoli, B. Akhmetov, Investigating the effects of integrating an absorption heat transformer with a combined cooling, heating and power system: A thermodynamic and economic analysis, Energy Convers. Manag. 228 (2021) 113677. https://doi.org/10.1016/j.enconman.2020.113677.

[27] R. Gomri, Thermal seawater desalination: Possibilities of using single effect and double effect absorption heat transformer systems, Desalination. 253 (2010) 112–118. https://doi.org/10.1016/j.desal.2009.11.023.

[28] S. Saren, S. Mitra, T. Miyazaki, K.C. Ng, K. Thu, A novel hybrid adsorption heat transformer – multi-effect distillation (AHT-MED) system for improved performance and waste heat upgrade, Appl. Energy. 305 (2022) 117744. https://doi.org/10.1016/j.apenergy.2021.117744.

[29] G. Srinivas, S. Sekar, R. Saravanan, S. Renganarayanan, Studies on a water-based absorption heat transformer for desalination using MED, Desalin. Water Treat. 1 (2009) 75–81. https://doi.org/10.5004/dwt.2009.110.

[30] F. Salata, M. Coppi, A first approach study on the desalination of sea water using heat transformers powered by solar ponds, Appl. Energy. 136 (2014) 611–618. https://doi.org/10.1016/j.apenergy.2014.09.079.

[31] S. Sekar, R. Saravanan, Experimental studies on absorption heat transformer coupled distillation system, Desalination. 274 (2011) 292–301. https://doi.org/10.1016/j.desal.2011.01.064.

[32] R.J. Romero, A. Rodríguez-Martínez, Optimal water purification using low grade waste heat in an absorption heat transformer, Desalination. 220 (2008) 506–513. https://doi.org/10.1016/j.desal.2007.05.026.

[33] D. Colorado, N. Demesa, A. Huicochea, J.A. Hernández, Irreversibility analysis of the absorption heat transformer coupled to a single effect evaporation process, Appl. Therm. Eng. 92 (2016) 71–80. https://doi.org/10.1016/j.applthermaleng.2015.09.076.

[34] K. Parham, M. Yari, U. Atikol, Alternative absorption heat transformer configurations integrated with water desalination system, Desalination. 328 (2013) 74–82. https://doi.org/10.1016/j.desal.2013.08.013.

[35] M. Khamooshi, K. Parham, I. Roozbeh, H. Ensafisoroor, Applications of innovative configurations of double absorption heat transformers in water purification technology, Desalin. Water Treat. 57 (2016) 8204–8216. https://doi.org/10.1080/19443994.2015.1020511.

[36] A. Hamidi, K. Parham, U. Atikol, A.H. Shahbaz, A parametric performance analysis of single and multi-effect distillation systems integrated with open-cycle absorption heat transformers, Desalination. 371 (2015) 37–45. https://doi.org/10.1016/j.desal.2015.06.003.

[37] M. Khamooshi, K. Parham, F. Egelioglu, M. Yari, H. Salati, Simulation and optimization of novel configurations of triple absorption heat transformers integrated to a water desalination system, Desalination. 348 (2014) 39–48. https://doi.org/10.1016/j.desal.2014.06.006.

[38] X. Zhang, D. Hu, Z. Li, Performance analysis on a new multi-effect distillation combined with an open absorption heat transformer driven by waste heat, Appl. Therm. Eng. 62 (2014) 239–244. https://doi.org/10.1016/j.applthermaleng.2013.09.015.

[39] A. Huicochea, J. Siqueiros, Improved efficiency of energy use of a heat transformer using a water purification system, Desalination. 257 (2010) 8–15. https://doi.org/10.1016/j.desal.2010.02.040.

[40] S.M. Alelyani, N.W. Fette, E.B. Stechel, P. Doron, P.E. Phelan, Techno-economic analysis of combined ammonia-water absorption refrigeration and desalination, Energy

Convers. Manag. 143 (2017) 493–504. https://doi.org/10.1016/j.enconman.2017.03.085.

[41] H.K. Abdulrahim, M.A. Darwish, Thermal desalination and air conditioning using absorption cycle, Desalin. Water Treat. 55 (2015) 3310–3329. https://doi.org/10.1080/19443994.2014.939492.

[42] P. Dumka, R. Chauhan, D.R. Mishra, Experimental and theoretical evaluation of a conventional solar still augmented with jute covered plastic balls, J. Energy Storage. 32 (2020) 101874. https://doi.org/10.1016/j.est.2020.101874.

[43] P. Dumka, A. Sharma, Y. Kushwah, A.S. Raghav, D.R. Mishra, Performance evaluation of single slope solar still augmented with sand-filled cotton bags, J. Energy Storage. 25 (2019) 100888. https://doi.org/10.1016/j.est.2019.100888.

[44] P. Dumka, D.R. Mishra, Performance evaluation of single slope solar still augmented with the ultrasonic fogger, Energy. 190 (2020) 116398. https://doi.org/10.1016/j.energy.2019.116398.

[45] D.S. Ayou, G. Zaragoza, A. Coronas, Small-scale renewable polygeneration system for off-grid applications : Desalination , power generation and space cooling, Appl. Therm. Eng. 182 (2021) 116112. https://doi.org/10.1016/j.applthermaleng.2020.116112.

[46] Y. Wang, N. Lior, Proposal and analysis of a high-efficiency combined desalination and refrigeration system based on the LiBr-H2O absorption cycle-Part 1: System configuration and mathematical model, Energy Convers. Manag. 52 (2011) 220–227. https://doi.org/10.1016/j.enconman.2010.06.071.

[47] M. Mehrpooya, B. Ghorbani, S.S. Hosseini, Thermodynamic and economic evaluation of a novel concentrated solar power system integrated with absorption refrigeration and desalination cycles, Energy Convers. Manag. 175 (2018) 337–356. https://doi.org/10.1016/j.enconman.2018.08.109.

[48] R. Beniwal, K. Garg, S.K. Das, H. Tyagi, Parametric analysis between closed air open water (CAOW) and closed water open air (CWOA) HDH cycles, 5-6th Therm. Fluids Eng. Conf. (2021) 447–455. https://doi.org/10.1615/tfec2021.ens.036676.

[49] F.A. Al-Sulaiman, M.I. Zubair, M. Atif, P. Gandhidasan, S.A. Al-Dini, M.A. Antar, Humidification dehumidification desalination system using parabolic trough solar air collector, Appl. Therm. Eng. 75 (2015) 809–816. https://doi.org/10.1016/j.applthermaleng.2014.10.072.

[50] H. Xu, X.Y. Sun, Y.J. Dai, Thermodynamic study on an enhanced humidification-dehumidification solar desalination system with weakly compressed air and internal heat recovery, Energy Convers. Manag. 181 (2019) 68–79. https://doi.org/10.1016/j.enconman.2018.11.073.

[51] N.A.A. Qasem, S.M. Zubair, A.M. Abdallah, M.H. Elbassoussi, M.A. Ahmed, Novel and efficient integration of a humidification-dehumidification desalination system with an absorption refrigeration system, Appl. Energy. 263 (2020). https://doi.org/10.1016/j.apenergy.2020.114659.

[52] K.M. Chehayeb, G.P. Narayan, S.M. Zubair, J.H. Lienhard, Thermodynamic balancing of a fixed-size two-stage humidification dehumidification desalination system, Desalination. 369 (2015) 125–139. https://doi.org/10.1016/j.desal.2015.04.021.

[53] Z. Rahimi-Ahar, M.S. Hatamipour, Y. Ghalavand, Solar assisted modified variable pressure humidification-dehumidification desalination system, Energy Convers. Manag. 162 (2018) 321–330. https://doi.org/10.1016/j.enconman.2018.01.063.

[54] E.A. S.A., R. Sathyamurthy, M.M. A., Improvement of humidification–dehumidification desalination unit using a desiccant wheel, Chem. Eng. Res. Des. 131 (2018) 104–116. https://doi.org/10.1016/j.cherd.2017.06.004.

[55] K. Srithar, T. Rajaseenivasan, Performance analysis on a solar bubble column humidification dehumidification desalination system, Process Saf. Environ. Prot. 105 (2017) 41–50. https://doi.org/10.1016/j.psep.2016.10.002.

[56] Y. Zhao, H. Zheng, S. Liang, N. Zhang, X. long Ma, Experimental research on four-stage cross flow humidification dehumidification (HDH) solar desalination system with direct contact dehumidifiers, Desalination. 467 (2019) 147–157. https://doi.org/10.1016/j.desal.2019.06.003.

[57] Z. Rahimi-Ahar, M.S. Hatamipour, Y. Ghalavand, Experimental investigation of a solar vacuum humidification-dehumidification (VHDH) desalination system, Desalination. 437 (2018) 73–80. https://doi.org/10.1016/j.desal.2018.03.002.

[58] N.A.S. Elminshawy, F.R. Siddiqui, M.F. Addas, Development of an active solar humidification-dehumidification (HDH) desalination system integrated with geothermal energy, Energy Convers. Manag. 126 (2016) 608–621. https://doi.org/10.1016/j.enconman.2016.08.044.

[59] S.M. Zubair, M.A. Antar, S.M. Elmutasim, D.U. Lawal, Performance evaluation of humidification-dehumidification (HDH) desalination systems with and without heat recovery options: An experimental and theoretical investigation, Desalination. 436 (2018) 161–175. https://doi.org/10.1016/j.desal.2018.02.018.

[60] S. Tangellapalli, Humidification-dehumidification and heat pump integration for water purifier and air conditioning, Energy Convers. Manag. 244 (2021) 114472. https://doi.org/10.1016/j.enconman.2021.114472.

[61] A. Fouda, S.A. Nada, H.F. Elattar, An integrated A/C and HDH water desalination system assisted by solar energy: Transient analysis and economical study, Appl. Therm. Eng. 108 (2016) 1320–1335. https://doi.org/10.1016/j.applthermaleng.2016.08.026.

[62] H.F. Elattar, A. Fouda, S.A. Nada, Performance investigation of a novel solar hybrid air conditioning and humidification-dehumidification water desalination system, Desalination. 382 (2016) 28–42. https://doi.org/10.1016/j.desal.2015.12.023.

[63] U. Sahoo, R. Kumar, P.C. Pant, R. Chaudhary, Development of an innovative polygeneration process in hybrid solar-biomass system for combined power, cooling and desalination, Appl. Therm. Eng. 120 (2017) 560–567. https://doi.org/10.1016/j.applthermaleng.2017.04.034.

[64] C. Chiranjeevi, T. Srinivas, Combined two stage desalination and cooling plant, Desalination. 345 (2014) 56–63. https://doi.org/10.1016/j.desal.2014.04.023.

[65] S. Marale, C. Chiranjeevi, T. Srinivas, R. ThundilKaruppa Raj, Experimental and Computational Fluid Dynamics Studies on Dehumidifier in a Combined Cooling and Desalination Plant, J. Therm. Sci. Eng. Appl. 9 (2017). https://doi.org/10.1115/1.4034596.

[66] A.M. Shaaban, M.A. Antar, A.E. Khalifa, M.A. El-Shaarawi, Analysis of Integrated H2O–LiBr Absorption Cooling and Single-Effect Evaporation Desalination System, Arab. J. Sci. Eng. 45 (2020) 5273–5284. https://doi.org/10.1007/s13369-020-04374-0.

[67] K. Garg, V. Khullar, S.K. Das, H. Tyagi, Parametric study of the energy efficiency of the HDH desalination unit integrated with nanofluid-based solar collector, J. Therm. Anal. Calorim. 135 (2019) 1465–1478. https://doi.org/10.1007/s10973-018-7547-6.

[68] D.W. Sun, Thermodynamic design data and optimum design maps for absorption refrigeration systems, Appl. Therm. Eng. 17 (1997) 211–221. https://doi.org/10.1016/s1359-4311(96)00041-5.

[69] J. Pátek, J. Klomfar, Simple functions for fast calculations of selected thermodynamic properties of the ammonia-water system, Int. J. Refrig. 18 (1995) 228–234. https://doi.org/10.1016/0140-7007(95)00006-W.

[70] K.E. Herold, R. Radermacher, S.A. Klein, Absorption Chillers and Heat Pumps, CRC Press, 2016. https://doi.org/10.1201/b19625.

[71] G.P. Narayan, M.H. Sharqawy, J.H. Lienhard V, S.M. Zubair, Thermodynamic analysis of humidification dehumidification desalination cycles, Desalin. Water Treat. 16 (2010) 339–353. https://doi.org/10.5004/dwt.2010.1078.

[72] A.K.S. Al-Sayyab, J. Navarro-Esbrí, A. Mota-Babiloni, Energy, exergy, and environmental (3E) analysis of a compound ejector-heat pump with low GWP refrigerants for simultaneous data center cooling and district heating, Int. J. Refrig. 133 (2022) 61–72. https://doi.org/10.1016/j.ijrefrig.2021.09.036.

[73] M. Dixit, A. Arora, S.C. Kaushik, Thermodynamic and thermoeconomic analyses of two stage hybrid absorption compression refrigeration system, Appl. Therm. Eng. 113 (2017) 120–131. https://doi.org/10.1016/j.applthermaleng.2016.10.206.

[74] F. Cudok, N. Giannetti, J.L.C. Ciganda, J. Aoyama, P. Babu, A. Coronas, T. Fujii, N. Inoue, K. Saito, S. Yamaguchi, F. Ziegler, Absorption heat transformer - state-of-the-art of industrial applications, Renew. Sustain. Energy Rev. 141 (2021). https://doi.org/10.1016/j.rser.2021.110757.

[75] R.M. Lazzarin, A. Gasparella, G.A. Longo, Ammonia-water absorption machines for refrigeration: Theoretical and real performances, Int. J. Refrig. 19 (1996) 239–246. https://doi.org/10.1016/0140-7007(96)00016-3.

[76] G.P. Narayan, M.H. Sharqawy, J.H. Lienhard V, S.M. Zubair, Thermodynamic analysis of humidification dehumidification desalination cycles, Desalin. Water Treat. 16 (2010) 339–353. https://doi.org/10.5004/dwt.2010.1078.

[77] G. Prakash Narayan, M.G. St. John, S.M. Zubair, J.H. Lienhard, Thermal design of the humidification dehumidification desalination system: An experimental investigation, Int. J. Heat Mass Transf. 58 (2013) 740–748. https://doi.org/10.1016/j.ijheatmasstransfer.2012.11.035.